The Astrophysical Journal, 785:63 (13pp), 2014 April 10 doi:10.1088/0004-637X/785/1/63


# ROTATION CURVE OF THE MILKY WAY OUT TO ∼200 kpc

Pijushpani Bhattacharjee[1,2], Soumini Chaudhury[2], and Susmita Kundu[2]
[1] McDonnell Center for the Space Sciences and Department of Physics, Washington University in St. Louis, Campus Box 1105, One Brookings Drive, St. Louis, MO 63130, USA; pijush.bhattacharjee@saha.ac.in
[2] AstroParticle Physics and Cosmology Division and Centre for AstroParticle Physics, Saha Institute of Nuclear Physics, 1/AF Bidhannagar, Kolkata 700064, India; soumini.chaudhury@saha.ac.in, susmita.kundu@saha.ac.in
*Received 2013 October 18; accepted 2014 February 16; published 2014 March 26*

## ABSTRACT

The rotation curve (RC) of our Galaxy, the Milky Way, is constructed starting from its very inner regions (few hundred parsecs) out to a large galactocentric distance of ∼200 kpc using kinematical data on a variety of tracer objects moving in the gravitational potential of the Galaxy, without assuming any theoretical models of the visible and dark matter (DM) components of the Galaxy. We study the effect on the RC due to the uncertainties in the values of the Galactic constants (GCs) $R_0$ and $V_0$ (these being the Sun's distance from and circular rotation speed around the Galactic center, respectively) and the velocity anisotropy parameter $\beta$ of the halo tracer objects used for deriving the RC at large galactocentric distances. The resulting RC in the disk region is found to depend significantly on the choice of the GCs, while the dominant uncertainty in the RC at large distances beyond the stellar disk comes from the uncertainty in the value of $\beta$. In general we find that the mean RC steadily declines at distances beyond ∼60 kpc, independently of the value of $\beta$. Also, at a given radius, the circular speed is lower for larger values of $\beta$ (i.e., for more radially biased velocity anisotropy). Considering that the largest possible value of $\beta$ is unity, which corresponds to stellar orbits being purely radial, our results for the case of $\beta = 1$ give a lower limit to the total mass of the Galaxy within ∼200 kpc, $M(200\,\mathrm{kpc}) \gtrsim (6.8 \pm 4.1) \times 10^{11}\ M_\odot$, independently of any model of the DM halo of the Galaxy.

*Key words:* dark matter – Galaxy: general – Galaxy: kinematics and dynamics

*Online-only material:* color figures, machine-readable table

## 1. INTRODUCTION

The circular velocity, $V_c(r) = \sqrt{GM(r)/r}$, of a test particle at a radial distance $r$ from the center of a mass distribution gives a direct measure of the total gravitational mass, $M(r)$, contained within that radius. A measured profile of $V_c$ as a function of $r$ for a spiral galaxy—often simply called its rotation curve (RC)—is therefore a direct probe of the spatial distribution of the total gravitating mass inside the galaxy including its dark matter (DM) content; see, e.g., Sofue & Rubin (2001) and Trimble (1987) for reviews. Recent comprehensive discussions of the RC and mass models for our Galaxy, the Milky Way, can be found, e.g., in Weber & de Boer (2010), Sofue (2012), and Nesti & Salucci (2013).

Recently, it has been shown that the RC of the Milky Way can be directly used to derive not only the local density of DM but also the velocity distribution of the DM particles in the Galaxy (Bhattacharjee et al. 2013), which are crucial for analyzing the results of both direct as well as indirect DM search experiments (Jungman et al. 1996); see also Cowsik et al. (2007), Chaudhury et al. (2010), Kundu & Bhattacharjee (2012), and Burch & Cowsik (2013). For this purpose, it is essential to derive the RC of the Galaxy to as large a galactocentric distance as possible without referring to any specific model of the DM halo of the Galaxy. In this paper we derive the RC of the Galaxy spanning a large range of galactocentric distances starting from its inner regions (∼0.2 kpc) out to ∼200 kpc using kinematical data on a variety of tracer objects moving in the gravitational potential of the Galaxy, without assuming any model of the DM halo of the Galaxy.

The circular velocity of a test particle in the Galaxy is, of course, not a directly measured quantity. The RC of the Galaxy has to be derived from the kinematical as well as positional data for an appropriate set of tracer objects moving in the gravitational field of the Galaxy. Except in few cases, the full three-dimensional velocity information of the tracers is not available, and the RC has to be reconstructed from only the measured line-of-sight (LOS) velocity and positional information of various tracer objects in the Galaxy.

For deriving the RC in the disk region of the Galaxy, one usually makes the reasonable assumption that the disk tracer objects move in circular orbits around the Galactic center. From the observed heliocentric LOS velocities, $v_h$, of the tracers and their position coordinates in the Galaxy, and with an assumed set of values of the Galactic constants (GCs), $[R_0, V_0]$, where $R_0$ and $V_0$ are the Sun's distance from and circular rotation speed around the Galactic center, respectively, that define the local standard of rest (LSR) frame, and by applying corrections for the peculiar motion of the Sun with respect to the LSR, one can obtain the circular velocities around the Galactic center, $V_c$, in a fairly straightforward manner (Binney & Merrifield 1998). Observations on a variety of tracers, such as H I regions, CO emission associated with H II regions, compact objects like Carbon stars (C stars), Cepheids, planetary nebulae (PNe), masers, and so on, have been used to derive the RC of the Galaxy in the disk region. Some recent compilations of RC data for the disk region of the Galaxy can be found, e.g., in Sofue et al. (2009) and Burch & Cowsik (2013).

To derive the RC in the outer regions of the Galaxy beyond the Galactic disk, one has to rely on distant tracers like blue horizontal branch (BHB) stars, K-giant (KG) stars, and relatively rare tracer objects like globular clusters (GCl), dwarf spheroidal (dSph) galaxies, and so forth, which populate the Milky Way's extended DM halo out to galactocentric distances of several hundreds of kiloparsecs. Unlike the disk tracers, these non-disk tracers do not exhibit any systematic motion,

and they move about in the Galaxy along various different orbits. The standard approach then is to assume that the tracer population under consideration is isotropically distributed in the halo of the Galaxy and then use the Jeans equation (Binney & Tremaine 2008) for spherical systems relating the circular velocity $V_c$ at radius $r$ to the number density and galactocentric radial as well as transverse velocity dispersions of the tracers at that radius. Of course, in the absence of full three-dimensional velocity information, with only the observed radial velocity dispersion available, the RC constructed using the Jeans equation depends on the unknown velocity anisotropy parameter $\beta \equiv 1 - \sigma_t^2/2\sigma_r^2$ (where $\sigma_r$ and $\sigma_t$ are the radial and transverse velocity dispersions of the tracers, respectively; see Section 3 below).

The Jeans equation approach has been used in several recent studies to extend the RC of the Galaxy to distances beyond the extent of the Galaxy's stellar disk. Accurate measurements of LOS velocities of a sample of 2401 BHB stars drawn from SDSS DR6 (Adelman-McCarthy et al. 2008) were used by Xue et al. (2008) to derive the RC of the Galaxy to ∼60 kpc for two constant ($r$-independent) values of $\beta$, namely $\beta = 0$ (isotropic velocity distribution) and $\beta = 0.37$, with the latter derived from results of numerical simulations. More recently, the Jeans equation has also been employed, together with certain analytical models of the phase-space distribution function of the tracer population, to construct the RC of the Galaxy to various distances of ∼25 to ∼80 kpc (Gnedin et al. 2010; Deason et al. 2012a; Kafle et al. 2012).

A crucial ingredient in the derivation of the distant RC using the Jeans equation is the measured radial velocity dispersion of the tracers as a function of their galactocentric distance $r$. An important finding in this regard is the result, first shown by Battaglia et al. (2005), that the radial velocity dispersion remains almost constant at a value of $\sim 120\,\mathrm{km\,s^{-1}}$ out to ∼30 kpc and then steadily *declines* down to a value of $\sim 50\,\mathrm{km\,s^{-1}}$ at $r \sim 120$ kpc. In their work, Battaglia et al. (2005) used a heterogeneous sample of about 240 halo objects consisting of field blue horizontal branch (FBH) stars, red giant stars, globular clusters, and distant satellite galaxies. A similar trend of the radial velocity dispersion profile has been found in several subsequent studies by using different samples of tracers, e.g., by Xue et al. (2008), Brown et al. (2010), Gnedin et al. (2010), Deason et al. (2012a), Deason et al. (2012b), and most recently in large cosmological simulations by Rashkov et al. (2013).

In this paper, we consider a combination of currently available large samples of a variety of both disk and non-disk tracers to construct the RC of the Galaxy from ∼0.2 kpc to ∼200 kpc. We perform a detailed analysis of the dependence of the RC on the choice of the GCs and also the dependence on the anisotropy parameter $\beta$ of the non-disk tracers. We find that while the RC in the disk region is significantly influenced by the choice of the GCs, the dominant uncertainty in the RC at large distances beyond the stellar disk comes from the uncertainty in the value of $\beta$. Since currently not much reliable observational information on $\beta$ is available, in this paper we calculate the circular velocities using the Jeans equation with the velocity anisotropy $\beta$ of the tracers taken as (1) a radially constant free parameter varying over a possible range of values from $\beta = 0$ (corresponding to complete isotropy of the tracers' orbits) to $\beta = 1$ (corresponding to completely radial orbits of the tracers), (2) a radially varying $\beta$ of the Osipkov–Merritt (OM) form (see Binney & Tremaine 2008, pp. 297–298) given by $\beta(r) = (1 + r_a^2/r^2)^{-1}$, where $r_a$ is the "anisotropy radius," and (3) a radial profile of $\beta$ obtained from recent large high-resolution hydrodynamical simulations of formation of late-type spirals like our Galaxy (Rashkov et al. 2013).

We find that irrespective of the value of $\beta$, the mean RC steadily declines with $r$ beyond $r \sim 60$ kpc. The circular speed at a given radius decreases as $\beta$ is increased (i.e., as the tracers' orbits are made more radially biased). Thus, the lowest value of the rotation speed at any $r$ obtains for the case of complete radial anisotropy ($\beta = 1$) of the non-disk tracers. This fact allows us to set a lower limit on the total mass of the Galaxy, $M(r)$, within a radius $r$, giving $M(200\,\mathrm{kpc}) \geqslant (6.8 \pm 4.1) \times 10^{11}\ M_\odot$. In this context, it may be noted that the recent numerical simulation study of Rashkov et al. (2013) indicates an increasingly radially biased velocity ellipsoid of the Galaxy's stellar population at large distances, with stellar orbits tending to be purely radial ($\beta \to 1$) beyond ∼100 kpc. If this behavior of $\beta$ is confirmed by future observational data, then the above lower limit on the Galaxy's mass (obtained from our results with $\beta = 1$) may in fact be a good estimate of the actual mass of the Galaxy out to ∼200 kpc.

The rest of this paper is arranged as follows. In Section 2 we derive the RC on the disk of the Galaxy up to a distance of ∼20 kpc from the Galactic center. We specify the various tracer samples used in our derivation of the RC and study the dependence of the RC on the chosen set of values of the GCs, $[R_0, V_0]$. In Section 3 we extend the RC to larger distances (up to ∼200 kpc) by an extensive analysis of various non-disk tracer samples discussed there in details. Finally, in Section 4, we present our unified RC and our estimates of the total mass of the Galaxy within ∼200 kpc and conclude by summarizing our main results in Section 5.

## 2. ROTATION CURVE FROM DISK TRACERS

Let us consider a tracer object with Galactic coordinates $(l, b)$ at a heliocentric distance $r_\mathrm{h}$ and observed heliocentric LOS velocity $v_h$ (see Figure 1).

We shall assume that the tracer follows a nearly circular orbit about the Galactic center. The velocity of the tracer as would be measured by an observer stationary with respect to the LSR, $v_\mathrm{LSR}$, can be obtained from the measured $v_h$ through the relation

$$v_\mathrm{LSR} = v_\mathrm{h} + U_\odot \cos b \cos l + V_\odot \cos b \sin l + W_\odot \sin b\,, \quad (1)$$

where $(U_\odot, V_\odot, W_\odot)$ denote the peculiar motion of the Sun with respect to LSR; see Figure 1. In our calculations below we shall take $(U_\odot, V_\odot, W_\odot) = (11.1, 12.24, 7.25)$ $(\mathrm{km\,s^{-1}})$ (Schönrich et al. 2010). Simple algebraic steps then allow us to relate the desired circular velocity with respect to Galactic center rest frame, $V_c$, to $v_\mathrm{LSR}$ as (Binney & Merrifield 1998)

$$V_c(R) = \frac{R}{R_0}\left[\frac{v_\mathrm{LSR}}{\sin l \cos b} + V_0\right], \quad (2)$$

where $R$ is the projection of the galactocentric distance $r$ onto the equatorial plane,

$$R = \sqrt{R_0^2 + r_\mathrm{h}^2 \cos^2 b - 2R_0 r_\mathrm{h} \cos b \cos l}\,. \quad (3)$$

For a given set of GCs, $[R_0, V_0]$, the Cartesian coordinates of the tracer are given by

$$\begin{aligned} x &= r_\mathrm{h} \cos b \sin l\,, \\ y &= R_0 - r_\mathrm{h} \cos b \cos l\,, \\ z &= r_\mathrm{h} \sin b\,, \end{aligned} \quad (4)$$

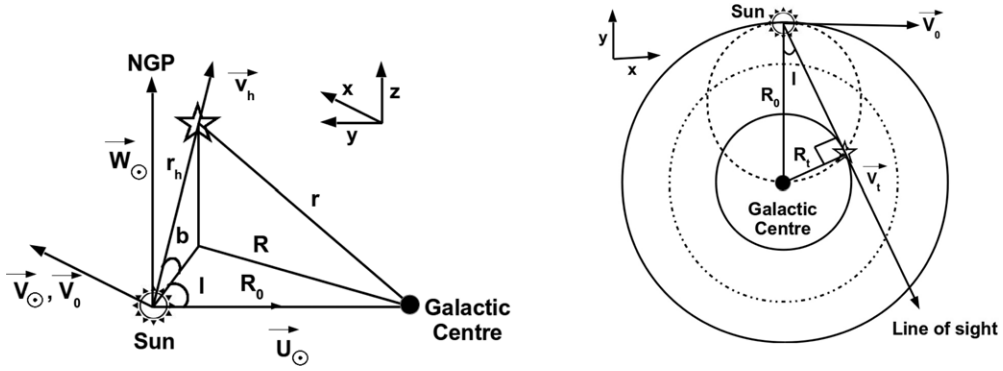


**Figure 1.** Left: schematic diagram showing the coordinate system, velocity and distance notations used in this work. Right: illustration of the tangent point method for deriving the circular speeds for distances $R < R_0$ on the disk.

with the Galactic center at the origin and the Sun lying on the Galactic mid-plane ($z = 0$) with coordinates $(x, y, z) = (0, R_0, 0)$ as illustrated in the left panel of Figure 1. Hence, for known $(l, b, r_{\rm h}, v_{\rm h})$ one can solve for $V_c$ from Equation (2) for a given set of GCs.

*Tangent Point Method*: For $R < R_0$, one can calculate $V_c$ by the simple tangent point method (Binney & Merrifield 1998) as follows: along a given LOS, the maximum LOS velocity will occur for the tracer closest to the Galactic center, with the LOS tangent to the circular orbit of the tracer at that point (see right panel of Figure 1). This maximum LOS velocity, called the terminal velocity ($v_t$), is easily seen to be related to $V_c$ through the relation

$$V_c(R_t) = |v_{t,\rm LSR}(R_t) + V_0 \sin l|, \quad (b = 0), \tag{5}$$

where

$$R_t = |R_0 \sin l| \tag{6}$$

is the distance of the tangent point from the Galactic center, and $v_{t,\rm LSR}$ is the $v_t$ corrected for the Sun's peculiar motion as in Equation (1).

For non-zero galactic latitude ($b$), Equation (5) generalizes to

$$V_c(R_t) = \left| \frac{v_{t,\rm LSR}(R_t)}{\cos b} + V_0 \sin l \right| , \tag{7}$$

and in this case the Cartesian coordinates of the tracer are given by

$$\begin{aligned} x &= R_0 \sin l \cos l \,, \\ y &= R_0 \sin^2 l \,, \\ z &= R_0 \cos l \tan b \,. \end{aligned} \tag{8}$$

Hence the circular velocity $V_c$ can be calculated directly from the measured terminal velocity by using Equation (7).

The details of the disk tracer samples used in this paper along with references to the corresponding data sources for each tracer genre are given in the Appendix (Table 3). The cuts on $l$ and $b$ are adopted from the published source papers. Toward the Galactic center ($l \to 0^\circ$) or anti-center ($l \to 180^\circ$), we expect $v_{\rm LSR}$ to approach zero to prevent unphysical $V_c$ values there (see Equation (2)). However, $v_{\rm LSR}$ observations in practice have finite values because of contamination from non-circular motions dominant there. Therefore, additional restrictions have been applied on $l$ ranges so as to ensure that we avoid observations too close to Galactic center (anti-center) regions. We further impose a cut to keep only the tracers whose $|z| \leqslant 2$ kpc and $R \leqslant 25$ kpc so as to ensure that the selected tracers "belong" to the stellar disk of the Galaxy. The $x$–$y$ and $l$–$z$ scatter plots for the selected disk tracers listed are shown in the Appendix (Figures 10 and 11, respectively).

It is clear from Equations (2)–(8) that the RC depends on the set of values of the GCs ($[R_0, V_0]$) adopted in the calculation. Values of $R_0$ in the range $\sim$(7–9) kpc and $V_0$ in the range $\sim$(180–250) km s$^{-1}$ exist in literature (see, e.g., Reid 1993; Olling & Merrifield 1998; Ghez et al. 2008; Reid et al. 2009; McMillan & Binney 2010; Sofue et al. 2011; Brunthaler et al. 2011; Schönrich 2012). Actually, the ratio $V_0/R_0 = (A - B)$, where $A$ and $B$ are the Oort constants (see, e.g., Binney & Merrifield 1998), is considerably better constrained. Maser observations and measurements of stellar orbits around Sgr A* near the Galactic center report values of $(A - B)$ in the range from about 29 to 32 km s$^{-1}$ kpc$^{-1}$ (Reid & Brunthaler 2004; Reid et al. 2009; McMillan & Binney 2010). RCs have been traditionally presented with the IAU recommended set of values, $[(R_0/\,{\rm kpc})\,, (V_0/\,{\rm km\,s^{-1}})]_{\rm IAU} = [8.5, 220]$, for which, however, the ratio $V_0/R_0 = 25.9$ is outside the range of values of this ratio mentioned above. A recently suggested set of values of $[R_0, V_0]$, consistent with observations of masers and stellar orbits around Sgr A* mentioned above, is $[(R_0/\,{\rm kpc})\,, (V_0/\,{\rm km\,s^{-1}})] = [8.3, 244]$ (see, e.g., Bovy et al. 2009; Gillessen et al. 2009).

In general, as easily seen from Equation (2), given a RC, $V_c(R)$, for a certain set of values of $[R_0, V_0]$, one can obtain the new RC, $\tilde{V}_c(R)$, for another set of values of the GCs denoted by $[\tilde{R}_0, \tilde{V}_0]$ through the relation

$$\tilde{V}_c(R) = \frac{R_0}{\tilde{R}_0} \left[ V_c(R) - \frac{R}{R_0}(V_0 - \tilde{V}_0) \right] . \tag{9}$$

In order to illustrate the dependence of the RC on the choice of the GCs, in this paper we shall calculate RCs with three different sets of values of $[(R_0/\,{\rm kpc})\,, (V_0/\,{\rm km\,s^{-1}})]$, namely the set [8.3, 244] mentioned above as well as two other sets—the IAU recommended set [8.5, 220] and the set [8.0, 200] (Sofue 2012).

Figure 2 shows our calculated RCs for the disk region of the Galaxy. The left panel of Figure 2 shows the RCs for each of the different tracer samples listed for the GCs set $[(R_0/\,{\rm kpc})\,, (V_0/\,{\rm km\,s^{-1}})] = [8.3, 244]$, and the right panel shows the RCs obtained by taking the weighted averages of the combined $V_c$ data from all the samples shown in the left panel, for three different sets of values of the GCs as indicated.

The circular velocities and their errors for individual disk tracer samples displayed in the left panel of Figure 2 are obtained in the following way: for each tracer object in a given sample we calculate $V_c$ and $R$ for the object from the known position

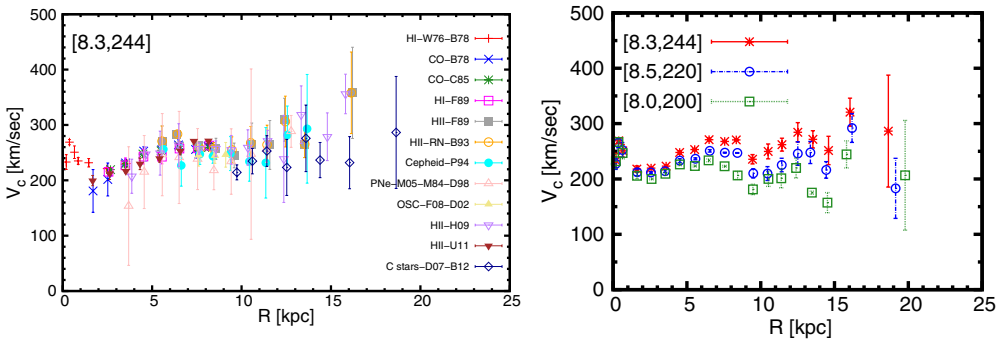


**Figure 2.** Left: rotation curves of the Galaxy obtained using the various different disk tracer samples listed in Table 3 in the Appendix for the Galactic constants $[(R_0/\,\mathrm{kpc})\,,(V_0/\,\mathrm{km\,s^{-1}})] = [8.3, 244]$. See Table 3 in the Appendix for keys to the data points. Right: averaged rotation curves obtained by weighted averaging over the combined $V_c$ data from all the disk tracer samples listed in Table 3 and shown in the left panel, for three different sets of values of $[(R_0/\,\mathrm{kpc})\,,(V_0/\,\mathrm{km\,s^{-1}})]$ as indicated.

(A color version of this figure is available in the online journal.)

coordinates of the object and its measured LOS velocity as described above. We then bin the resulting data ($V_c$ vs. $R$) in $R$, and in each $R$ bin we calculate the mean of all the $V_c$ values of all the objects contained within that bin and assign it to the mean $R$ value of the objects in that bin. The error bars on $V_c$ correspond simply to the standard deviation of the $V_c$ values in that bin.[3] We have taken a bin size of 0.25 kpc for $0 < R \leqslant 1$ kpc, 1.0 kpc for $1 < R \leqslant 15$ kpc, and 2.5 kpc for $15 < R \leqslant 17.5$ kpc. The objects with $R > 17.5$ kpc are few in number and are placed in one single bin. The above choices of the bin widths in $R$ for various ranges of $R$, arrived at by trial and error, are "optimal" in the sense that the bin widths are large enough so that there are a sufficient number of objects in each bin (to allow the mean value of $V_c$ in the bin to be a reasonably good representative of the true value of $V_c$ at the value of $R$ under consideration), while at the same time being not too large as to miss the fine features of the RC. The RCs in the right panel of Figure 2 are obtained by combining the $V_c$ data from all the samples shown in the left panel in the same $R$ bins as above and then calculating the mean circular speed ($V_c$) and its $1\sigma$ uncertainty ($\Delta V_c$) within each bin by the standard weighted average method (Bevington & Robinson 2003):

$$V_c = \frac{\sum_i w_i V_{c,i}}{\sum_i w_i}\,, \quad \text{and} \quad \Delta V_c = \sqrt{\frac{1}{\sum_i w_i}}\,, \tag{10}$$

with $w_i = 1/(\Delta V_{c,i})^2$, where $V_{c,i}$ and $\Delta V_{c,i}$ are the $V_c$ value and its $1\sigma$ error, respectively, of the $i$th data point within the bin.

As seen from Figure 2, the RC in the disk region depends significantly on the choice of GCs. As expected, at any given $R$ the circular velocity is higher for a higher value of $V_0$.

## 3. ROTATION CURVE FROM NON-DISK TRACERS

In order to extend the RC beyond the Galactic disk, we next consider tracer objects populating the stellar halo of the Galaxy. Unlike the nearly circularly rotating disk tracers, the non-disk tracers do not exhibit any systematic circular motion. Hence the formalism described in the previous section cannot be used to derive the RC at large galactocentric distances beyond the Galactic disk. Instead, we use the Jeans equation (see, e.g., Binney & Tremaine 2008, pp. 349) for spherical systems relating the number density and radial as well as transverse velocity dispersions of the tracers at radius $r$ to the circular velocity $V_c$ at that radius:

$$V_c^2(r) = \frac{GM(r)}{r} = -\sigma_r^2\left(\frac{d\ln n_{\rm tr}}{d\ln r} + \frac{d\ln\sigma_r^2}{d\ln r} + 2\beta\right)\,. \tag{11}$$

Here $r = (R_0^2 + r_{\rm h}^2 - 2R_0 r_{\rm h}\cos b\cos l)^{1/2}$ is the galactocentric radial distance of a tracer (see Figure 1), and $n_{\rm tr}$, $\sigma_r$ and $\beta$ are, respectively, the number density of the tracer population, their galactocentric radial velocity dispersion, and the velocity anisotropy parameter, at $r$. The velocity anisotropy $\beta$ is defined as

$$\beta = 1 - \frac{\sigma_t^2}{2\sigma_r^2}\,, \tag{12}$$

where $\sigma_t$ is the galactocentric transverse velocity dispersion of the tracers.

In this work, we have chosen two independent classes of non-disk stellar tracers, namely, a sample of 4985 BHB stars from SDSS-DR8 compiled by Xue et al. (2011) and a set of 4781 KG stars from SDSS-DR9 (Xue et al. 2014). These two samples allow us to probe the Galactic halo up to a galactocentric distance of ~100 kpc. In order to reach out further we consider an additional heterogeneous (Hg) sample of 430 objects comprising 143 GCl (Harris 1996, 2010), 118 red halo giants (Carney et al. 2003, 2008), 108 FHB stars (Clewley et al. 2004), 38 RR-Lyrae stars (Kinman et al. 2012), and 23 dSph (McConnachie 2012). To ensure that the sample comprises of only halo objects, we apply a cut on the $z$ and $R$ coordinates of the tracers, leaving out objects with $r < 25$ kpc in all the non-disk tracer samples mentioned above. After these cuts, we are left with a "BHB" sample of 1457 BHB stars, a "KG" sample of 2227 KG stars, and a "Hg" sample of 65 objects comprising 16 GCls, 28 FHB stars, and 21 dSphs, with which we shall construct our RC for the non-disk region. The last sample allows us to extend the RC to a galactocentric distance of 190 kpc, the mean $r$ of the objects in the furthest radial bin in the Hg sample. The spatial distributions of the three final non-disk tracer samples (after position cuts mentioned above) in terms of $x$–$z$, $y$–$z$, and $x$–$y$ scatter plots are shown in the Appendix (Figure 12).

The number density of the tracers, $n_{\rm tr}$, appearing in the Jeans equation (11) is estimated in the following way. We radially bin the objects in a given sample, estimate the tracer density from the star counts in the annular volume of each bin, and assign it at the mean radius of the objects contained within that bin. In order to

[3] Note that the LOS velocities $v_h$ of individual tracer objects are measured fairly accurately and their measurement errors contribute negligibly little to the final errors on the $V_c$ values.

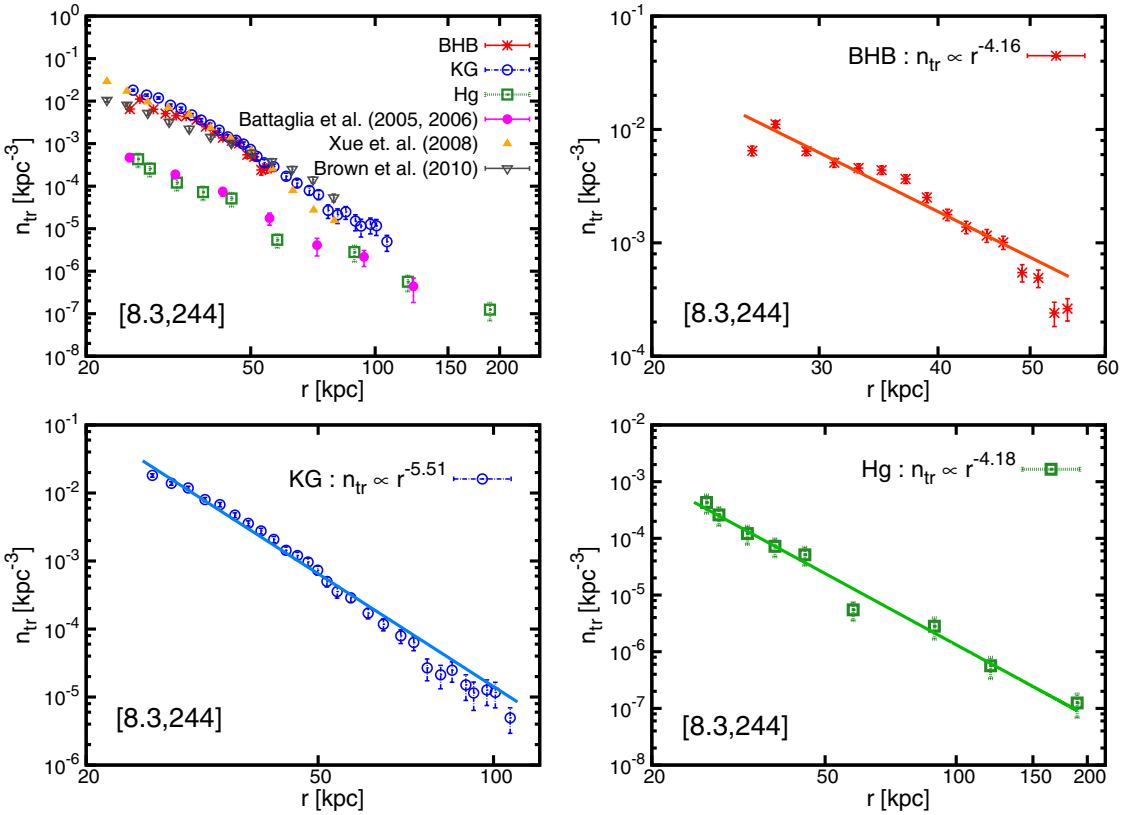


**Figure 3.** Tracer number density, $n_{\rm tr}$, for the three non-disk tracer samples considered in this paper (see the text and Figure 12 in the Appendix for details and source references for the samples). The top left panel shows, for comparison, the tracer densities obtained in some earlier studies (Battaglia et al. 2005; Xue et al. 2008; Brown et al. 2010) which used different tracer samples. The other three panels show the best power law fits to the radial profiles of $n_{\rm tr}$ for the three non-disk samples. The GC set used is $[(R_0/\,{\rm kpc})\,,(V_0/\,{\rm km\,s^{-1}})] = [8.3,\,244]$.

(A color version of this figure is available in the online journal.)

ensure a reasonably good number of objects per bin, we adopt a variable bin size increasing with distance. For the BHB sample, a uniform bin size of 2 kpc is used over its entire range of $r$ from 25 to 55 kpc. For the KG samples, the bin widths are 2 kpc for $25\,{\rm kpc} < r \leqslant 55\,{\rm kpc}$ and 4 kpc for $55\,{\rm kpc} < r \leqslant 103\,{\rm kpc}$; objects with $r > 103$ kpc (up to 110 kpc) are all placed in one single bin. For the Hg sample, because of the relatively small total number (65) of objects, we adopt the following optimal, "object wise" binning in increasing order of the galactocentric distance $r$ of the objects: the first six radial bins contain eight objects in each bin; the next two bins contain six objects in each bin; and, finally, the remaining five objects are placed in one single bin. Uncertainties in the number density estimates are obtained from Poissonian errors on the tracer counts in each bin.

The resulting density estimates for the three samples mentioned above with the GCs set $[(R_0/\,{\rm kpc})\,,(V_0/\,{\rm km\,s^{-1}})] = [8.3,\,244]$ are shown in Figure 3, where we also show for comparison (see the top left panel of Figure 3) the tracer densities from some earlier studies that used different tracer samples. Our results are seen to be in reasonably good agreement with those obtained in the previous studies.

We then perform power law fits ($n_{\rm tr}(r) \propto r^{-\gamma}$) to the radial profile of the tracer number density for each of the three samples separately. The resulting best power law fits are also shown in Figure 3. The values of the parameters of the best power law fit for each tracer sample are given in Table 1. Within each sample, there is no significant difference in the values of $n_{\rm tr}$ for the three different sets of GCs, as also seen from the values of the power law fit parameters given in Table 1.

**Table 1**
Number Densities and Radial Velocity Dispersions of Non-disk Tracers

| $\left[\frac{R_0}{\rm kpc}\,,\,\frac{V_0}{\rm km\,s^{-1}}\right]$ | $n_{\rm tr} = n_0\,(\frac{r}{50\,{\rm kpc}})^{-\gamma}\,,\ \sigma_{\rm GSR} = \sigma_0\,(\frac{r}{50\,{\rm kpc}})^{-\alpha}$ | | | |
|---|---|---|---|---|
| | $\frac{n_0}{\rm kpc^3}$ | $\gamma$ | $\frac{\sigma_0}{\rm km\,s^{-1}}$ | $\alpha$ |
| | BHB | | | |
| [8.3, 244] | $7.51 \times 10^{-4}$ | 4.16 | 93.0 | 0.06 |
| [8.5, 220] | $7.66 \times 10^{-4}$ | 4.15 | 94.45 | 0.07 |
| [8.0, 200] | $7.45 \times 10^{-4}$ | 4.17 | 93.58 | 0.05 |
| | KG | | | |
| [8.3, 244] | $6.57 \times 10^{-4}$ | 5.51 | 86.75 | 0.31 |
| [8.5, 220] | $6.53 \times 10^{-4}$ | 5.51 | 88.23 | 0.30 |
| [8.0, 200] | $6.40 \times 10^{-4}$ | 5.51 | 87.89 | 0.29 |
| | Hg | | | |
| [8.3, 244] | $2.37 \times 10^{-5}$ | 4.18 | 121.21 | 0.37 |
| [8.5, 220] | $2.39 \times 10^{-5}$ | 4.18 | 117.51 | 0.40 |
| [8.0, 200] | $2.38 \times 10^{-5}$ | 4.17 | 115.34 | 0.42 |

**Notes.** Given are the best-fit parameter values for power-law fits to the radial profiles of the number density, $n_{\rm tr}$, and the galactic standard of rest (GSR) frame LOS velocity dispersion, $\sigma_{\rm GSR}$, of the tracers for the three non-disk tracer samples considered in this paper (see text and Figure 12 in the Appendix for details and source references for the samples). The parameter values are given for three different sets of values of the GCs, $[(R_0/\,{\rm kpc})\,,(V_0/\,{\rm km\,s^{-1}})]$.

Next, we have to calculate the galactocentric radial velocity dispersion, $\sigma_r$, that appears in the Jeans equation (11), for our non-disk samples. To do this we first transform the observed heliocentric LOS velocity, $v_h$, of each individual tracer object

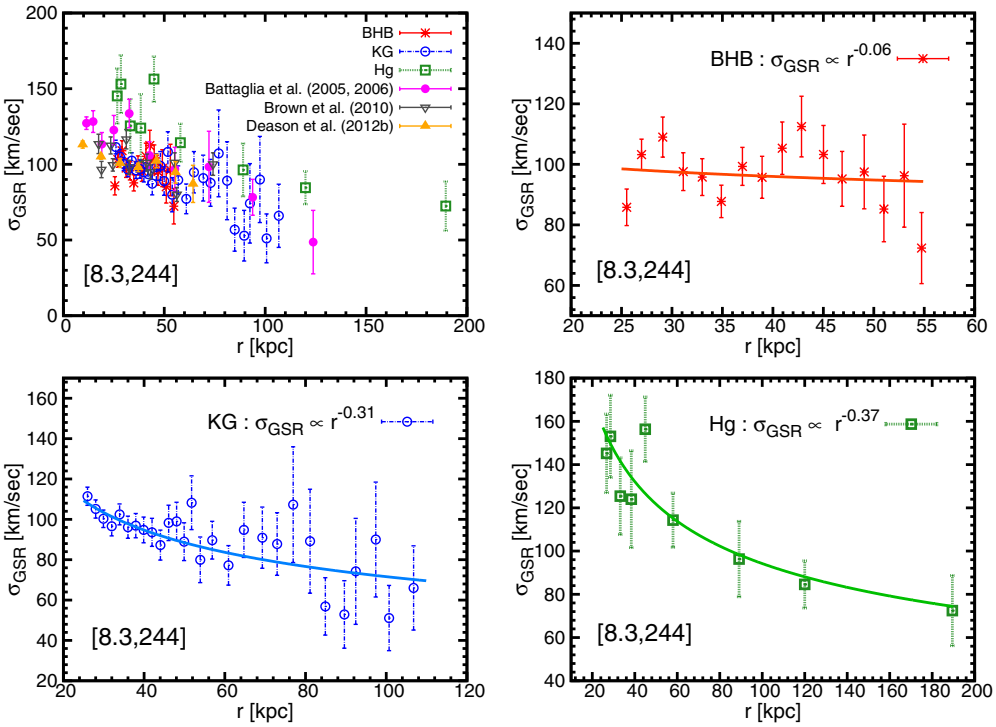


**Figure 4.** GSR frame LOS velocity dispersion of the tracers, $\sigma_{\rm GSR}$, for the three non-disk tracer samples considered in this paper (see the text and Figure 12 in the Appendix for details and source references for the samples). The top left panel also shows, for comparison, the $\sigma_{\rm GSR}$ obtained in some earlier studies (Battaglia et al. 2005; Brown et al. 2010; Deason et al. 2012b) which used different tracer samples. The other three panels show the best power law fits to the radial profiles of $\sigma_{\rm GSR}$ for the three non-disk samples. The GC set used is $[(R_0/\,{\rm kpc})\,,(V_0/\,{\rm km\,s^{-1}})] = [8.3, 244]$.

(A color version of this figure is available in the online journal.)

to $v_{\rm GSR}$, the velocity that would be measured in the Galactic standard of rest (GSR) frame. This is easily done by correcting for the circular motion of the LSR ($V_0$) and solar peculiar motion with respect to LSR, ($U_\odot$, $V_\odot$, $W_\odot$) (see Figure 1):

$$v_{\rm GSR} = v_{\rm h} + U_\odot \cos b \cos l + V_\odot \cos b \sin l + W_\odot \sin b + V_0 \cos b \sin l\,. \quad (13)$$

For large samples like the BHB and KG stars described above, we calculate the $v_{\rm GSR}$ for all the individual tracers in the same radial bins as used in the estimation of the tracers' number density described above, calculate their dispersion, $\sigma_{\rm GSR}$, and assign it to the mean radius of all the tracers contained within that bin. The corresponding uncertainty, $\Delta\sigma_{\rm GSR}$, in our estimate of $\sigma_{\rm GSR}$ in each bin is calculated by using the standard formula $\Delta\sigma_{\rm GSR} = \sqrt{1/[2(N-1)]}\sigma_{\rm GSR}$ (Lehmann & Castella 1998; Evans et al. 1993; Graham et al. 1994), where $N$ is the number of objects in the bin.

For the Hg sample, however, owing to its small size, we follow a different method, similar to that used in Battaglia et al. (2005), for calculating the $\sigma_{\rm GSR}$ and its uncertainty in each radial bin: we randomly generate a sample of 10,000 mock values of $v_h$ for each tracer object in a radial bin using a Gaussian centered at the observed value of $v_h$ and a width of typically ∼(10–20)% of this $v_h$ value. We then transform these 10,000 $v_h$ values for each tracer in the bin to get the corresponding 10,000 values of $v_{\rm GSR}$ using Equation (13), and we calculate the associated dispersions $\sigma_{\rm GSR}$ in that bin. We assign the mean value of the $\sigma_{\rm GSR}$ values for all the objects in a given bin to the mean radius of all the objects in the bin. The corresponding uncertainty in $\sigma_{\rm GSR}$ is taken to be the rms deviation of the $\sigma_{\rm GSR}$ values in that bin.

Our results for $\sigma_{\rm GSR}$ for the three tracer samples are shown in Figure 4, in which we also show for comparison (see the top left panel of Figure 4) the $\sigma_{\rm GSR}$ values obtained in some earlier studies using different samples, which, again, are seen to be in reasonably good agreement with our results.

The other three panels of Figure 4 show the best power law fits ($\sigma_{\rm GSR}(r) \propto r^{-\alpha}$) to the radial profiles of $\sigma_{\rm GSR}$ for each of the three non-disk samples. The values of the parameters of the best power law fits for the three tracer samples are given in Table 1. Again, as in the case of $n_{\rm tr}$, the effect of variation of the GCs on $\sigma_{\rm GSR}$ is negligible.

Finally, the galactocentric radial velocity dispersion, $\sigma_r$, can be obtained from $\sigma_{\rm GSR}$ by using the relation (Battaglia et al. 2005)

$$\sigma_r = \frac{\sigma_{\rm GSR}}{\sqrt{1-\beta H(r)}}\,, \quad (14)$$

where

$$H(r) = \frac{r^2+R_0^2}{4r^2} - \frac{\left(r^2-R_0^2\right)^2}{8r^3R_0}\ln\frac{r+R_0}{r-R_0}\,, \quad (r > R_0) \quad (15)$$

and $\beta$ is the velocity anisotropy of the tracers defined in Equation (12). Equation (14) is derived by decomposing the $v_{\rm GSR}$'s into their galactocentric radial and transverse components and taking the averages of the squares of the velocity components.[4]

The last quantity that remains to be specified before we can solve the Jeans equation (11) is the velocity anisotropy parameter, $\beta$, of the tracers. There is not much definite observational information available on the value of $\beta$ of the tracers because

[4] Note that Equation (3) given in the 2005 paper of Battaglia et al. (2005) is incorrect. The correct equation, same as Equation (14) above, is given in the 2006 (Erratum) paper of Battaglia et al. (2005) and also in Dehnen et al. (2006).

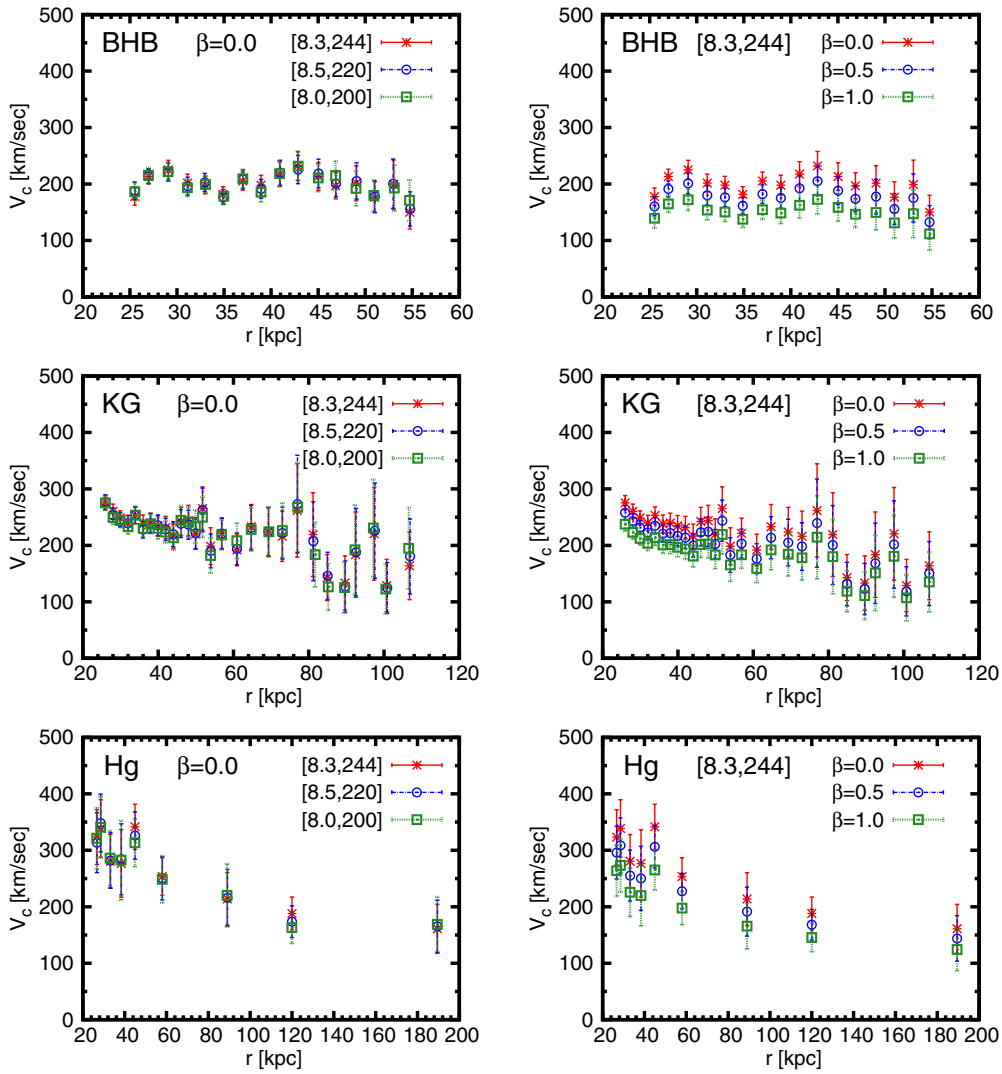


**Figure 5.** Circular velocities with their $1\sigma$ error bars for the three different non-disk tracer samples used in this paper (see the text and Figure 12 in the Appendix for details and source references for the samples). The left panels are for tracer velocity anisotropy $\beta = 0$ and three different sets of values of the Galactic constants, $[(R_0/\,\mathrm{kpc})\,,(V_0/\,\mathrm{km\,s^{-1}})]$, as indicated, whereas the right panels show the results for three different constant ($r$-independent) values of $\beta = 0$, 0.5 and 1, with $[(R_0/\,\mathrm{kpc})\,,(V_0/\,\mathrm{km\,s^{-1}})] = [8.3, 244]$.

(A color version of this figure is available in the online journal.)

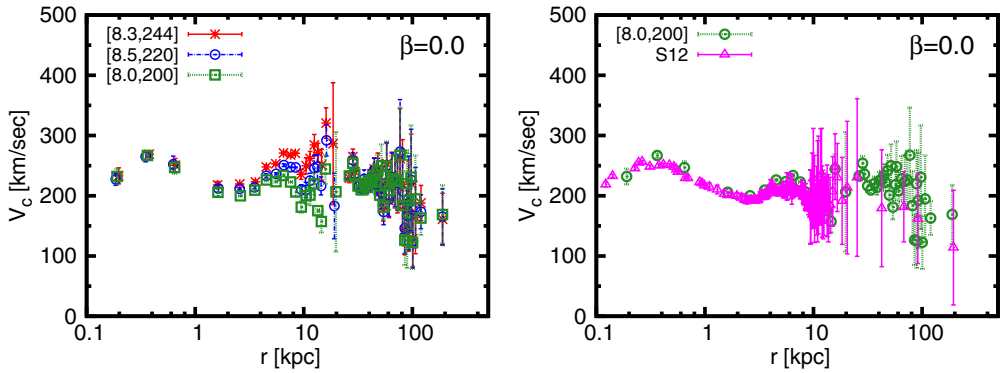


**Figure 6.** Left: rotation curve of the Galaxy for three different sets of values of the Galactic constants $[(R_0/\,\mathrm{kpc})\,,(V_0/\,\mathrm{km\,s^{-1}})]$ as indicated and non-disk tracers' velocity anisotropy parameter $\beta = 0$. The data points and their $1\sigma$ error bars shown here are obtained by weighted averaging over the combined $V_c$ data obtained from different disk and non-disk tracer samples (see Figures 2 and 5). Right: rotation curve of the Galaxy for $[(R_0/\,\mathrm{kpc})\,,(V_0/\,\mathrm{km\,s^{-1}})] = [8.0, 200]$ and non-disk tracers' velocity anisotropy parameter $\beta = 0$ compared with that obtained by Sofue (2012; S12).

(A color version of this figure is available in the online journal.)

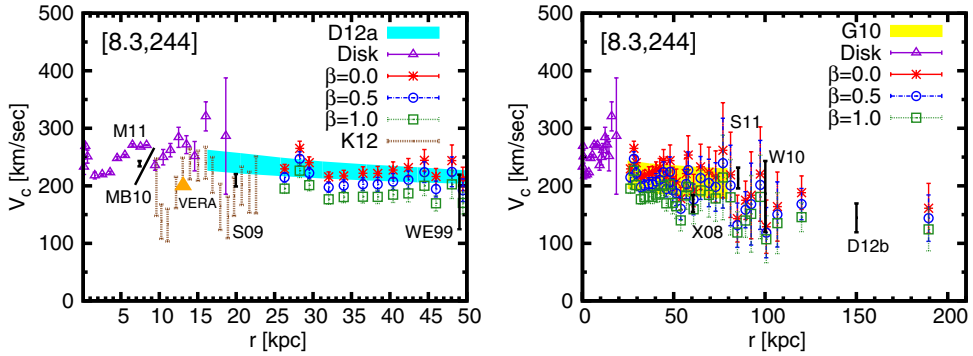


**Figure 7.** Rotation Curve for $[(R_0/\,\mathrm{kpc})\,,(V_0/\,\mathrm{km\,s^{-1}})] = [8.3, 244]$ and various values of $\beta$. The shaded bands marked D12a and G10 in the left and right panels, respectively, represent the RCs and their uncertainty bands obtained earlier by Deason et al. (2012a; D12a; up to $r \sim 50$ kpc) and Gnedin et al. (2010; G10; up to $r \sim 80$ kpc), respectively. In addition, estimates of circular velocities at certain specific values of $r$ obtained from various independent considerations by Kafle et al. (2012; K12), McMillan (2011; M11), McMillan & Binney (2010; MB10), Honma et al. (2007; VERA), Sofue et al. (2009; S09), Wilkinson & Evans (1999; WE99), Xue et al. (2008; X08), Samurovic et al. (2011; S11), Watkins et al. (2010; W10), and Deason et al. (2012b; D12b) are shown for comparison.

(A color version of this figure is available in the online journal.)

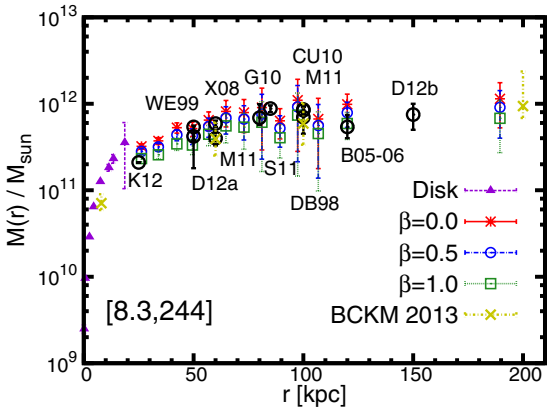


**Figure 8.** Mass, $M(r) = rV_c^2(r)/G$, within $r$, as a function of $r$, obtained from the RCs shown in Figure 7 for $[(R_0/\,\mathrm{kpc})\,,(V_0/\,\mathrm{km\,s^{-1}})] = [8.3, 244]$ and various values of the tracers' velocity anisotropy parameter $\beta$. Estimates of $M(r)$ at certain specific values of $r$ obtained from various independent considerations in some earlier works, namely, Kafle et al. (2012; K12), Wilkinson & Evans (1999; WE99), Deason et al. (2012a; D12a), Xue et al. (2008; X08), McMillan (2011; M11), Gnedin et al. (2010; G10), Samurovic et al. (2011; S11), Catena & Ullio (2010; CU10), Dehnen & Binney (1998; DB98), Battaglia et al. (2005; B05-06), Deason et al. (2012b; D12b), and Bhattacharjee et al. (2013; BCKM 2013), are shown for comparison.

(A color version of this figure is available in the online journal.)

of the lack of availability of proper motion measurements on a sufficiently large number of tracer objects. In general $\beta$ can be a function of $r$. A recent maximum likelihood analysis (Deason et al. 2012a) of radial velocity data of a large sample of halo stars, performed within the context of a model for the (in general anisotropic) velocity distribution function of the halo stars, indicates the stellar velocity anisotropy being radially biased with a value of $\beta \sim 0.5$ for $r$ from ~16 kpc up to $r \sim 48$ kpc. This is also indicated by the recent results from the large numerical simulation study of Rashkov et al. (2013), which finds the velocity distribution of the Galaxy's stellar population at large $r$ to be radially biased ($\beta > 0$) with stellar orbits tending to purely radial ($\beta \to 1$) at $r \gtrsim 100$ kpc. On the basis of these considerations, to explore various possibilities for $\beta$, in this paper we shall calculate our RCs for (1) three representative constant values of $\beta$, namely, $\beta = 0$ (isotropic), 0.5 (mildly radially biased anisotropy), and 1 (fully radially anisotropic); (2) a radially varying $\beta$ of the OM form (see Binney & Tremaine 2008, pp. 297–298) given by $\beta(r) = (1 + r_a^2/r^2)^{-1}$, where $r_a$ is the "anisotropy radius"; and (3) a radial profile of $\beta$ obtained from the recent large high-resolution hydrodynamical simulations performed by Rashkov et al. (2013). In principle, $\beta$ and its radial profile may be different for different tracer samples. However, since currently no reliable measurements of $\beta$ for the different samples extending to large galactocentric distances are available, any choice of different $\beta$ for different samples would be necessarily arbitrary. For simplicity, therefore, we assume the same values of $\beta$ and its radial profile for our three tracer samples.

**Table 2**
Rotation Curve of the Milky Way

| $r$ (kpc) | $V_c$ ($\mathrm{km\,s^{-1}}$) | $\Delta V_c$ ($\mathrm{km\,s^{-1}}$) | $r$ (kpc) | $V_c$ ($\mathrm{km\,s^{-1}}$) | $\Delta V_c$ ($\mathrm{km\,s^{-1}}$) |
|---|---|---|---|---|---|
| 0.20 | 233.0 | 13.32 | 38.41 | 191.57 | 11.73 |
| 0.38 | 268.92 | 4.67 | 40.42 | 197.59 | 14.12 |
| 0.66 | 250.75 | 11.35 | 42.40 | 192.79 | 5.92 |
| 1.61 | 217.83 | 5.81 | 44.49 | 213.22 | 17.17 |
| 2.57 | 219.58 | 1.48 | 45.99 | 179.39 | 11.23 |
| 3.59 | 223.11 | 2.43 | 48.06 | 213.03 | 24.72 |
| 4.51 | 247.88 | 2.99 | 49.49 | 178.57 | 17.63 |
| 5.53 | 253.14 | 1.69 | 51.39 | 183.31 | 23.58 |
| 6.50 | 270.95 | 2.19 | 53.89 | 157.89 | 19.57 |
| 7.56 | 267.80 | 0.96 | 56.89 | 191.76 | 24.35 |
| 8.34 | 270.52 | 0.66 | 57.98 | 210.72 | 29.81 |
| 9.45 | 235.58 | 8.44 | 60.92 | 168.02 | 25.67 |
| 10.50 | 249.72 | 13.44 | 64.73 | 206.47 | 36.27 |
| 11.44 | 261.96 | 11.71 | 69.31 | 203.62 | 40.89 |
| 12.51 | 284.30 | 17.50 | 72.96 | 190.53 | 40.98 |
| 13.53 | 271.54 | 15.57 | 76.95 | 222.72 | 74.37 |
| 14.59 | 251.43 | 25.60 | 81.13 | 186.29 | 66.53 |
| 16.05 | 320.70 | 25.27 | 84.90 | 122.25 | 36.46 |
| 18.64 | 286.46 | 101.18 | 89.35 | 143.95 | 29.49 |
| 26.30 | 189.64 | 6.74 | 92.44 | 154.66 | 67.23 |
| 28.26 | 237.99 | 11.54 | 97.41 | 184.0 | 72.86 |
| 29.51 | 209.82 | 9.16 | 100.72 | 108.68 | 40.99 |
| 32.04 | 179.14 | 6.65 | 106.77 | 137.15 | 53.17 |
| 33.99 | 170.37 | 6.93 | 119.98 | 150.18 | 25.46 |
| 36.49 | 175.92 | 6.62 | 189.49 | 125.01 | 37.32 |

**Notes.** Given are the circular velocity, $V_c$, and its $1\sigma$ error, $\Delta V_c$, for various values of the galactocentric distance, $r$, for a radial profile of the non-disk tracers' velocity anisotropy parameter $\beta$ derived from Figure 2 of Rashkov et al. (2013), with $[(R_0/\,\mathrm{kpc})\,,(V_0/\,\mathrm{km\,s^{-1}})] = [8.3, 244]$.

(This table is available in its entirety in a machine-readable form in the online journal. A portion is shown here for guidance regarding its form and content.)

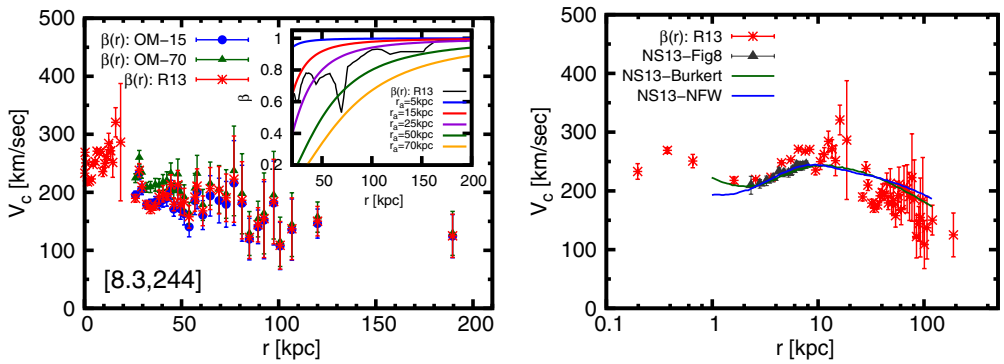


**Figure 9.** Left: rotation curve of the Milky Way to ∼200 kpc for $[(R_0/\,\mathrm{kpc})\,,(V_0/\,\mathrm{km\,s^{-1}})] = [8.3, 244]$ and for a radial profile of the non-disk tracers' velocity anisotropy parameter $\beta$ of the Osipkov–Merritt (OM) form, $\beta(r) = (1 + r_a^2/r^2)^{-1}$, with two values of the "anisotropy radius" $r_a$ =15 kpc (OM-15) and 70 kpc (OM-70). The RC data generated with a radial profile of $\beta$ derived from Figure 2 of Rashkov et al. (2013; R13; data points marked $\beta(r)$:R13) are also shown for comparison. The inset shows the OM $\beta$ profile for various values of $r_a$ together with the $\beta$ profile from Figure 2 of R13. Right: $\beta(r)$:R13 from the left panel but in log scale and compared with the circular velocity data from terminal velocities (NS13-Fig8) and rotation curve fits for Burkert (NS13-Burkert) and NFW (NS13-NFW) models from Nesti & Salucci (2013). The numerical data for $\beta(r)$:R13 and three sets of values of $[(R_0/\,\mathrm{kpc})\,,(V_0/\,\mathrm{km\,s^{-1}})] = [8.0,200]$, [8.3,244], and [8.5,220] are available in the online version of the paper in Table 2.

(A color version of this figure is available in the online journal.)

With $n_{\rm tr}$, $\sigma_r$ and $\beta$ thus specified, we can now proceed to solve the Jeans equation (11) to obtain the $V_c$ profiles for the three different tracer samples described above. For each tracer sample we calculate the $V_c$ values in the same radial bins as used in calculating the $n_{\rm tr}$ values and $\sigma_{\rm GSR}$ values, and the best-fit power law forms of $n_{\rm tr}$ and $\sigma_{\rm GSR}$ described above are used for calculating the radial derivatives appearing in the Jeans equation (11). The corresponding $1\sigma$ error, $\Delta V_c$, on $V_c$ within each radial bin is calculated from those of $n_{\rm tr}$ and $\sigma_{\rm GSR}$ in the bin by standard quadrature.

The resulting RCs for the three tracer samples are shown in Figure 5. As clear from the left panels of Figure 5, the RCs for different choices of GCs almost overlap, thus indicating that the RC at large galactocentric distances beyond a few tens of kiloparsec is fairly insensitive to the precise values of the GCs. Instead, the main uncertainty in the RC comes from the unknown value of the tracers' velocity anisotropy parameter $\beta$, as evident from the right panels of Figure 5. As expected, the lowest rotation speeds obtain for the most radially biased velocity anisotropy ($\beta = 1$).

## 4. COMBINED ROTATION CURVES TO $r \sim 200$ kpc

We now combine the RCs obtained from disk and non-disk tracers (Figures 2 and 5) to construct the RC of the Galaxy up to ∼200 kpc.

For the disk region ($r < 25$ kpc) we take the averaged $V_c$ data for a chosen set of GCs from the right panel of Figure 2. For the non-disk region ($r \geqslant 25$ kpc), we combine the $V_c$ data from Figure 5 for the three tracer samples in every 2 kpc radial bins and calculate the resulting mean circular speed ($V_c$) and its $1\sigma$ uncertainty ($\Delta V_c$) within a bin by weighted averaging as described in Section 2 (see Equation (10)).

The resulting RCs for $\beta = 0$ and three sets of values of the GCs are shown in Figure 6, and those for different values of $\beta$ for one particular set of GCs, $[(R_0/\,\mathrm{kpc})\,,(V_0/\,\mathrm{km\,s^{-1}})] = [8.3, 244]$, are shown in Figure 7. For comparison, we also show in Figure 7 estimates of circular velocities at specific values of $r$ obtained from a variety of independent considerations in some earlier studies by various authors.

The $\beta$ dependence of the radial profile of the cumulative mass, $M(r) = r\,V_c^2(r)/G$, is shown in Figure 8. Again, estimates of $M(r)$ from various independent considerations and given at certain specific values of $r$ in some earlier works, are also shown in Figure 8 for comparison.

Note that the lowest mass of the Galaxy corresponds to $\beta = 1$, which allows us to set a lower limit on the mass of the Galaxy, $M(\sim 200\,\mathrm{kpc}) \geqslant (6.8 \pm 4.1) \times 10^{11}\ M_\odot$.

In Figure 9 we show the full RC of the Galaxy out to ∼200 kpc for $[(R_0/\,\mathrm{kpc})\,,(V_0/\,\mathrm{km\,s^{-1}})] = [8.3, 244]$ and for a radial profile of the non-disk tracers' velocity anisotropy parameter $\beta$ of the OM form, $\beta(r) = (1 + r_a^2/r^2)^{-1}$, for two different values of $r_a = 15$ kpc and 70 kpc. In addition, we show the RC generated with a $\beta$ profile extracted from Figure 2 of Rashkov et al. (2013) with the corresponding numerical data in tabular form given in Table 2. The inset in the left panel of Figure 9 shows the OM $\beta$ profile for various values of $r_a$ as well as the $\beta$ profile obtained in Rashkov et al. (2013). The latter is seen to roughly follow the OM form and is reasonably well bracketed within OM $\beta$ profiles with $r_a = 15$ kpc and $r_a = 70$ kpc. In Figure 9 we also show the circular velocity data from terminal velocities and RC fits for the Burkert and Navarro–Frenk–White (NFW) models of the DM halo of the Galaxy given in Nesti & Salucci (2013) (up to ∼100 kpc) in comparison with our RC generated with the $\beta$ profile of Rashkov et al. (2013).

As already mentioned, a noticeable feature of the RC, irrespective of the velocity anisotropy of the tracer objects, is its clearly declining nature beyond about ∼60 kpc, as would be expected of an effectively finite size of the DM halo of the Galaxy.

We emphasize that for any given $\beta$, the RC and mass profile of the Galaxy shown in Figures 7 and 8, respectively, are based entirely on observational data and are obtained without making any models of the mass distributions of the various components (the bulge, disk, and DM halo) of the Galaxy.

## 5. SUMMARY

In this paper, we have constructed the RC of the Galaxy from a galactocentric distance of ∼0.2 kpc out to ∼200 kpc by using kinematical data on a variety of both disk and non-disk objects that trace the gravitational potential of the Galaxy, without assuming any theoretical models of the visible and DM components of the Galaxy. We have studied the dependence of the RC on the choice of the GCs and also studied the dependence

on the velocity anisotropy parameter $\beta$ of the non-disk tracers. The RC in the disk region is found to depend significantly on the choice of values of the GCs. The RC at large distances beyond the stellar disk, however, depends more significantly on the parameter $\beta$ than on the values of the GCs. In general, the mean RC is found to steadily decline beyond $r \sim 60$ kpc, irrespective of the value of $\beta$. At any given galactocentric distance $r$, the circular speed is lower for larger values of $\beta$. Considering that the largest allowed value of $\beta$ is unity (complete radial anisotropy), this allows us to set a model-independent lower limit on the total mass of the Galaxy, giving $M(\lesssim 200\,\mathrm{kpc}) \geqslant (6.8 \pm 4.1) \times 10^{11}\, M_{\odot}$. We have also noted that recent results from high-resolution hydrodynamical simulations of formation of galaxies like Milky Way (Rashkov et al. 2013) indicate an increasingly radially biased velocity ellipsoid of the Galaxy's stellar population at large distances, with stellar orbits tending to be almost purely radial ($\beta \to 1$) beyond ~100 kpc. This implies that the above lower limit on the Galaxy's mass (obtained from our results with $\beta = 1$) may in fact be a good estimate of the actual mass of the Galaxy out to ~200 kpc.

We thank G. Battaglia, W. Brown, A. Deason, O. Gnedin, P. Kafle, S. Sharma, Y. Sofue, M. Weber, and X. Xue for useful communications. P.B. thanks R. Cowsik for discussions and for support under a Clark Way Harrison Visiting Professorship at the McDonnell Center for the Space Sciences and Physics Department at Washington University in St. Louis. We thank the anonymous referee for useful comments and suggestions.

## APPENDIX

In this Appendix, we collect together some details of the disk and non-disk tracers used in this paper for calculating the RCs. These are given in Table 3 and Figures 10–12.

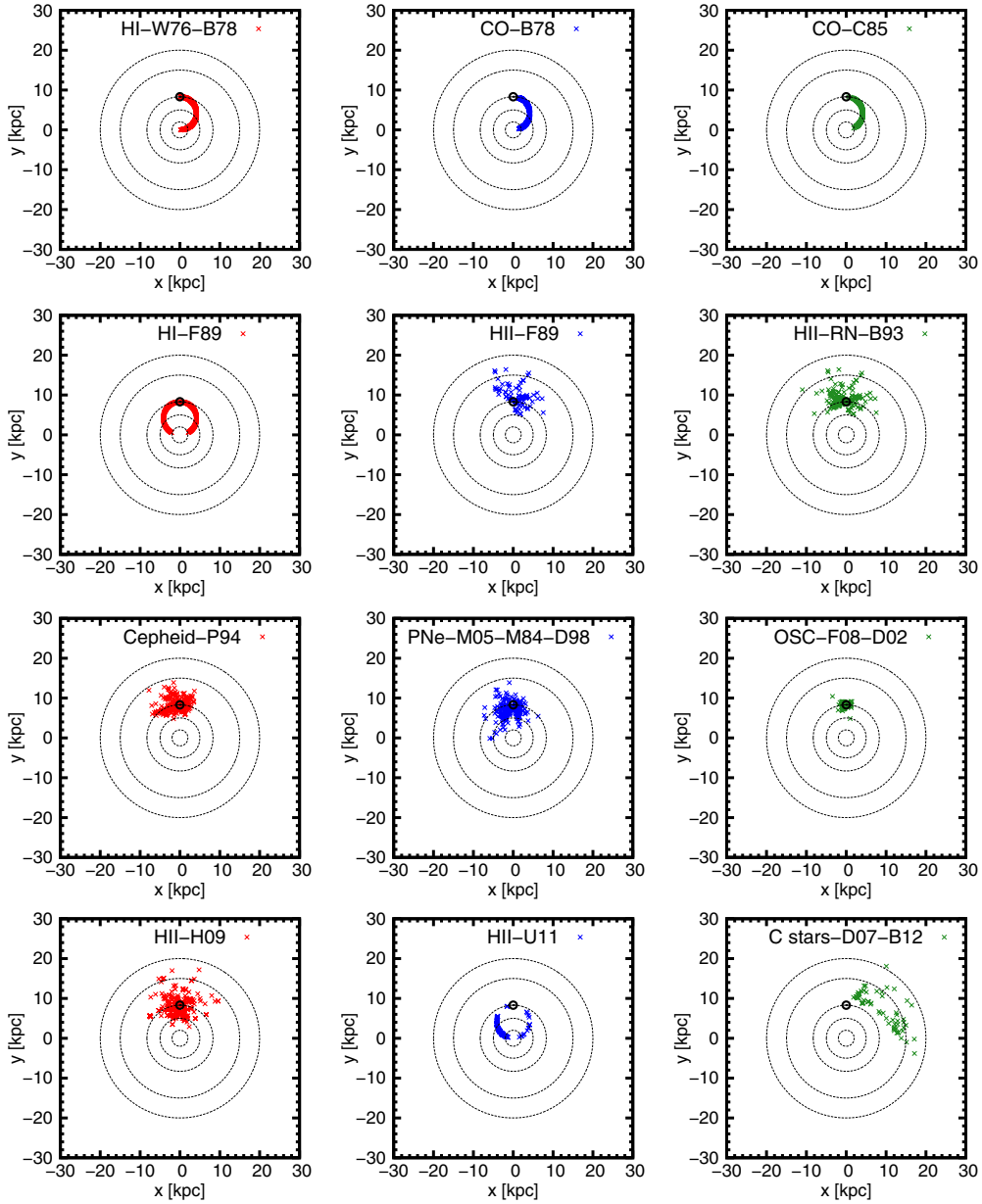


**Figure 10.** $x$–$y$ scatter plots for the different disk tracer samples listed in Table 3, for the case $R_0 = 8.3$ kpc. The Galactic center is chosen to be at origin (0, 0) with the Sun marked by an open circle located at (0, $R_0$).

(A color version of this figure is available in the online journal.)

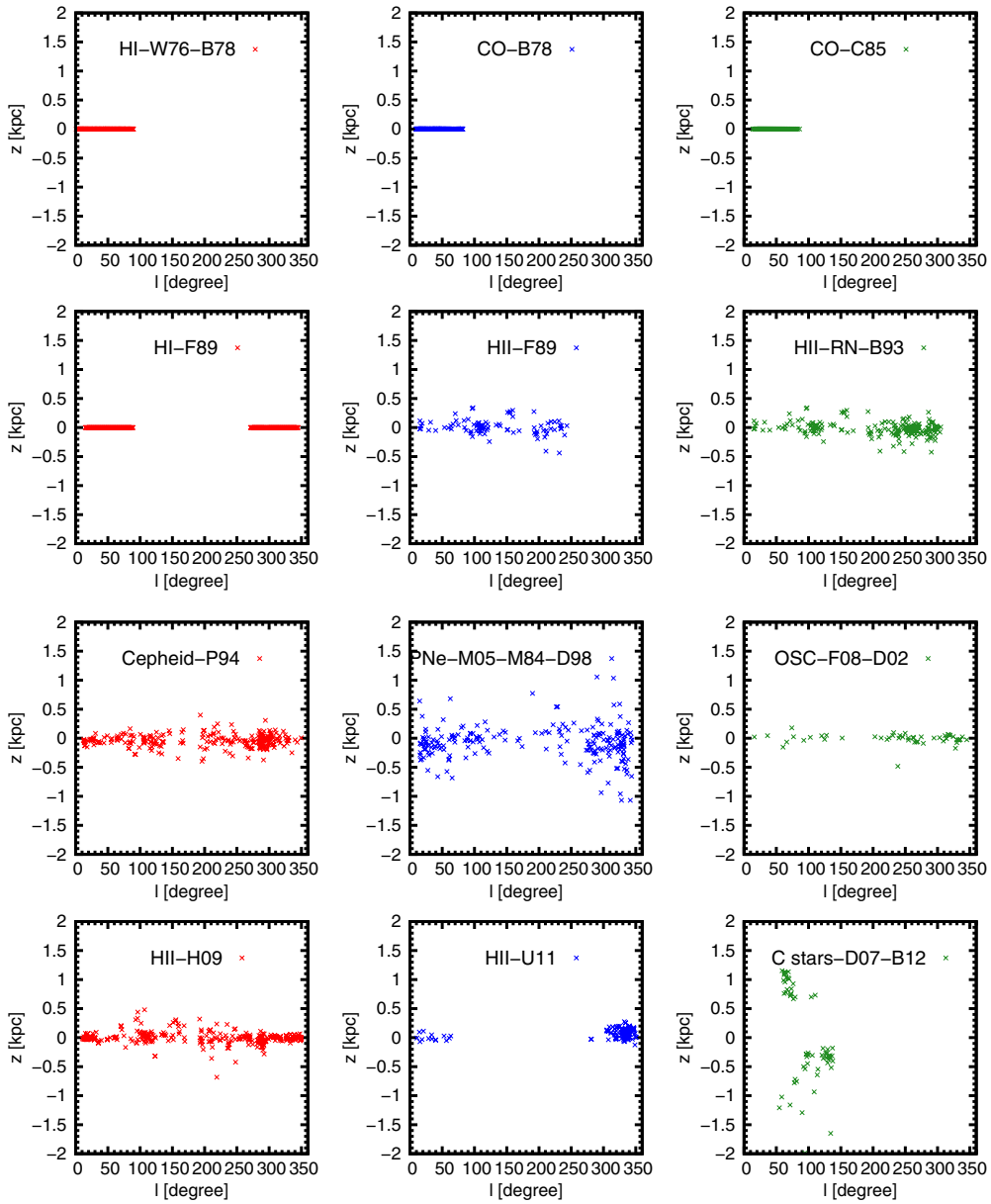


**Figure 11.** Galactic longitude, $l$, vs. height from Galactic mid-plane, $z$, for the different disk tracer samples listed in Table 3, for the case $R_0 = 8.3$ kpc. (A color version of this figure is available in the online journal.)

**Table 3**
Disk Tracer Types, Their Source References, and $(l, b)$ Ranges of the Data Sets used in This Paper

| Tracer Type | Data Source | $(l, b)$ Ranges |
|---|---|---|
| H I regions[a] (HI-W76-B78) | Westerhout (1976), Burton & Gordon (1978) | $1^\circ < l < 90^\circ$ |
| CO clouds[a] (CO-B78) | Burton & Gordon (1978) | $9^\circ < l < 82^\circ$ |
| CO clouds[a] (CO-C85) | Clemens (1985) | $13^\circ < l < 86^\circ$ |
| H I regions[a] (HI-F89) | Fich et al. (1989) | $15^\circ < l < 89^\circ$ and $271^\circ < l < 345^\circ$ |
| H II regions (HII-F89) | Fich et al. (1989) | $10^\circ < l < 170^\circ$ and $190^\circ < l < 350^\circ$ |
| H II regions and reflection nebulae (HII-RN-B93) | Brand & Blitz (1993) | $10^\circ < l < 170^\circ$ and $190^\circ < l < 350^\circ$ |
| Cepheids (Cepheid-P94) | Pont et al. (1994) | $10^\circ < l < 170^\circ$ and $190^\circ < l < 350^\circ$; $\lvert b\rvert < 10^\circ$ |
| Planetary nebulae (PNe-M05-M84-D98) | Maciel & Lago (2005), Maciel (1984), Durand et al. (1998) | $15^\circ < l < 345^\circ$; $\lvert b\rvert < 10^\circ$ |
| Open star clusters (OSC-F08-D02) | Frinchaboy & Majewski (2008), Dias et al. (2002) | $10^\circ < l < 170^\circ$ and $190^\circ < l < 350^\circ$; $\lvert b\rvert < 9^\circ$ |
| H II regions (HII-H09) | Hou et al. (2009) | $10^\circ < l < 170^\circ$ and $190^\circ < l < 350^\circ$ |
| H II regions[a] (HII-U11) | Urquhart et al. (2012) | $10^\circ < l < 65^\circ$ and $280^\circ < l < 350^\circ$ |
| C stars (C stars-D07-B12) | Demers & Battinelli (2007), Battinelli et al. (2013) | $54^\circ < l < 150^\circ$; $3^\circ < \lvert b\rvert < 9^\circ$ |

**Notes.** Superscript "a" denotes the tracers limited within the solar circle ($R < R_0$) where tangent point method has been used to derive the rotation speeds. The identifier for each tracer data set used in the paper is given within parentheses in the first column under the respective tracer type for subsequent references in the paper.

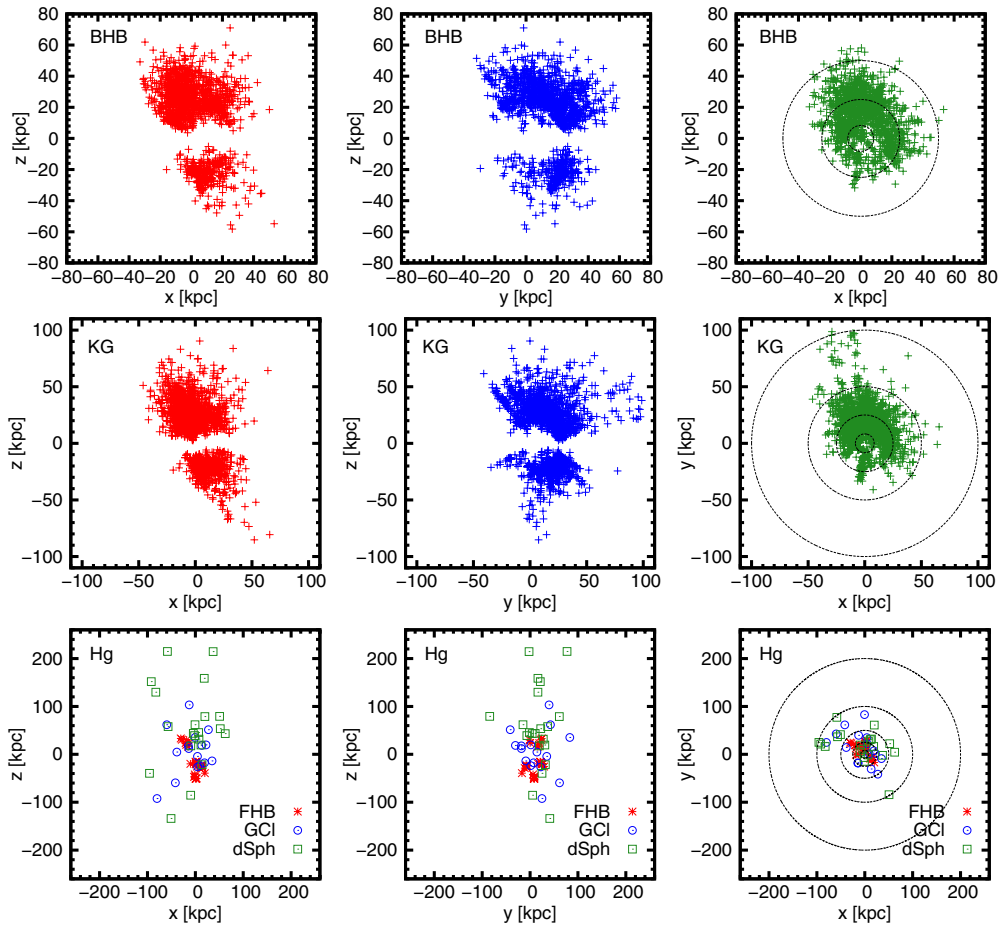


**Figure 12.** $x$–$z$, $y$–$z$ and $x$–$y$ scatter plots (after removing objects with $r < 25$ kpc; see text) for the three samples of non-disk tracer objects considered in this paper, namely, (1) the "BHB" sample, a set of 1457 blue horizontal branch stars from the compilation of Xue et al. (2011), (2) the "KG" sample, a set of 2227 K-giant stars from the compilation of Xue et al. (2014), and (3) the "Hg" sample, a heterogeneous set of 65 objects comprising of 16 globular clusters (GCl) from Harris (1996, 2010), 28 FHB stars from Clewley et al. (2004), and 21 dwarf spheroidals (dSph) from McConnachie (2012), for $R_0 = 8.3$ kpc with the Sun located at $(x = 0, y = R_0, z = 0)$.

(A color version of this figure is available in the online journal.)

## REFERENCES


Adelman-McCarthy, J. K., Agüeros, M. A., Allam, S. S., et al. 2008, ApJS, 175, 297

Battaglia, G., Helmi, A., Morrison, H., et al. 2005, MNRAS, 364, 433 (erratum 370, 1055 [2006])

Battinelli, P., Demers, S., Rossi, C., & Gigoyan, K. S. 2013, Ap, 56, 68

Bevington, P. R., & Robinson, D. K. 2003, Data Reduction and Error Analysis for the Physical Sciences (3rd ed.; New York: McGraw-Hill)

Bhattacharjee, P., Chaudhury, S., Kundu, S., & Majumdar, S. 2013, PhRvD, 87, 083525

Binney, J., & Merrifield, M. 1998, Galactic Astronomy (Princeton, NJ: Princeton Univ. Press)

Binney, J., & Tremaine, S. 2008, Galactic Dynamics (2nd ed.; Princeton, NJ: Princeton Univ. Press)

Bovy, J., Hogg, D. W., & Hans-Walter, R. 2009, ApJ, 704, 1704

Brand, J., & Blitz, L. 1993, A&A, 275, 67

Brown, W. R., Geller, M. J., Kenyon, S. J., & Diaferio, A. 2010, AJ, 139, 59

Brunthaler, A., Reid, M. J., Menten, K. M., et al. 2011, AN, 332, 461

Burch, B., & Cowsik, R. 2013, ApJ, 779, 35

Burton, W. B., & Gordon, M. A. 1978, A&A, 63, 7

Carney, B. W., Latham, D. W., Stefanik, R. P., & Laird, J. B. 2008, AJ, 135, 196

Carney, B. W., Latham, D. W., Stefanik, R. P., Laird, J. B., & Morse, J. A. 2003, AJ, 125, 293

Catena, R., & Ullio, P. 2010, JCAP, 08, 004

Chaudhury, S., Bhattacharjee, P., & Cowsik, R. 2010, JCAP, 09, 020

Clemens, D. P. 1985, ApJ, 295, 422

Clewley, L., Warren, S. J., Hewett, P. C., Norris, J. E., & Evans, N. W. 2004, MNRAS, 352, 285

Cowsik, R., Ratnam, C., Bhattacharjee, P., & Majumdar, S. 2007, NewA, 12, 507

Deason, A. J., Belokurov, V., Evans, N. W., & An, J. 2012a, MNRAS, 424, L44 (D12a)

Deason, A. J., Belokurov, V., Evans, N. W., et al. 2012b, MNRAS, 425, 2840 (D12b)

Dehnen, W., & Binney, J. 1998, MNRAS, 294, 429

Dehnen, W., McLaughlin, D. E., & Sachania, J. 2006, MNRAS, 369, 1688

Demers, S., & Battinelli, P. 2007, A&A, 473, 143

Dias, W. S., Alessi, B. S., Moitinho, A., & Lépine, J. R. D. 2002, A&A, 389, 871

Durand, S., Acker, A., & Zijlstra, A. 1998, A&AS, 132, 13

Evans, M., Hastings, N., & Peacock, B. 1993, Statistical Distributions (New York: Wiley)

Fich, M., Blitz, L., & Stark, A. A. 1989, ApJ, 342, 272

Frinchaboy, P. M., & Majewski, S. R. 2008, AJ, 136, 118

Ghez, A. M., Salim, S., Weinberg, N. N., et al. 2008, ApJ, 689, 1044

Gillessen, S., Eisenhauer, F., Trippe, S., et al. 2009, ApJ, 692, 1075

Gnedin, O. Y., Brown, W. R., Geller, M. J., & Kenyon, S. J. 2010, ApJL, 720, L108

Graham, R. L., Knuth, D. E., & Patashnik, O. 1994, Concrete Mathematics: A Foundation for Computer Science (Reading, MA: Addison-Wesley)

Harris, W. E. 1996, AJ, 112, 1487

Harris, W. E. 2010, arXiv:1012.3224

Honma, M., Bushimata, T., Choi, Y. K., et al. 2007, PASJ, 59, 839

Hou, L. G., Han, J. L., & Shi, W. B. 2009, A&A, 499, 473

Jungman, G., Kamionkowski, M., & Griest, K. 1996, PhR, 267, 195

Kafle, P. R., Sharma, S., Lewis, G. F., & Bland-Hawthorn, J. 2012, ApJ, 761, 98

Kinman, T. D., Cacciari, C., Bragaglia, A., Smart, R., & Spagna, A. 2012, MNRAS, 422, 2116

Kundu, S., & Bhattacharjee, P. 2012, PhRvD, 85, 123533
Lehmann, E. L., & Casella, G. 1998, Theory of Point Estimation (New York: Springer)
Maciel, W. J. 1984, A&AS, 55, 253
Maciel, W. J., & Lago, L. G. 2005, RMxAA, 41, 383
McConnachie, A. W. 2012, AJ, 144, 4
McMillan, P. J. 2011, MNRAS, 414, 2446
McMillan, P. J., & Binney, J. 2010, MNRAS, 402, 934
Nesti, F., & Salucci, P. 2013, JCAP, 07, 016
Olling, R. P., & Merrifield, M. R. 1998, MNRAS, 297, 943
Pont, F., Mayor, M., & Burki, G. 1994, A&A, 285, 415
Rashkov, V., Pillepich, A., Deason, A. J., et al. 2013, ApJ, 773, 32
Reid, M. J. 1993, ARA&A, 31, 345
Reid, M. J., & Brunthaler, A. 2004, ApJ, 616, 872
Reid, M. J., Menten, K. M., Zheng, X. W., et al. 2009, ApJ, 700, 137
Samurović, S., & Lalović, A. 2011, A&A, 531, A82
Schönrich, R. 2012, MNRAS, 427, 274
Schönrich, R., Binney, J., & Dehnen, W. 2010, MNRAS, 403, 1829
Sofue, Y. 2012, PASJ, 64, 75
Sofue, Y., Honma, M., & Omodaka, T. 2009, PASJ, 61, 227
Sofue, Y., Nagayama, T., Matsui, M., & Nakagawa, A. 2011, PASJ, 63, 867
Sofue, Y., & Rubin, V. 2001, ARA&A, 39, 137
Trimble, V. 1987, ARA&A, 25, 425
Urquhart, J. S., Hoare, M. G., Lumsden, S. L., et al. 2012, MNRAS, 420, 1656
Watkins, L. L., Evans, N. W., & An, J. H. 2010, MNRAS, 406, 264
Weber, M., & de Boer, W. 2010, A&A, 509, A25
Westerhout, G. 1976, Maryland-Bonn Galactic 21-cm Line Survey (College Park, Univ. Maryland)
Wilkinson, M. I., & Evans, N. W. 1999, MNRAS, 310, 645
Xue, X. X., Ma, Z., Rix, H. W., et al. 2014, ApJ, 784, 170
Xue, X. X., Rix, H. W., Yanny, B., et al. 2011, ApJ, 738, 79
Xue, X. X., Rix, H. W., Zhao, G., et al. 2008, ApJ, 684, 1143